

MIMO Radar Moving Target Detection in Homogeneous Clutter

Qian He, Nikolaus H. Lehmann, Rick S. Blum, *Fellow, IEEE*,
and Alexander M. Haimovich, *Senior Member, IEEE*,

Abstract

A multiple-input multiple-output (MIMO) radar approach employing widely-dispersed transmit and receive antennas is studied for the detection of moving targets. The MIMO approach transmits orthogonal waveforms from the different transmit antennas so these waveforms can be separated at each receive antenna. For a moving target in colored Gaussian noise-plus-clutter, we quantify the gains from having widely-dispersed antennas that allow the overall system to “view” the target simultaneously from several different directions. The MIMO radar performance is contrasted with that of a traditional phased-array approach, which employs closely-spaced antennas for this purpose. The MIMO radar approach is well suited to handle targets that have small radial velocities for scenarios in which co-located sensors cannot separate the target from the background clutter. Both a centralized processing and a simple distributed processing form of the MIMO radar approach are developed and studied, and the gains from the centralized version, which come at the price of additional complexity, are clearly demonstrated and explained intuitively. The constant false alarm rate property of an adaptive version of the MIMO moving target detector is also demonstrated for homogeneous clutter.

Index Terms

Moving target detection (MTD), centralized processing, multiple-input multiple-output (MIMO) radar.

Q. He is with the EE Department, University of Electronic Science and Technology of China, Chengdu, Sichuan 610054 China. This work was done while she was visiting Lehigh University (email: qih207@lehigh.edu).

R. S. Blum is with the ECE Department, Lehigh University, Bethlehem, PA 18015 USA (email: rblum@eecs.lehigh.edu).

N. H. Lehmann and A. M. Haimovich are with the ECE Department, New Jersey Institute of Technology, Newark, NJ 07102 USA (email: lehmann@njit.edu; haimovich@njit.edu).

Q. He’s work was supported by China Scholarship Council. R. S. Blum’s work was supported by the Air Force Research Laboratory under agreement No. FA9550-06-1-0041, the National Science Foundation under grant No. CCF-0829958, and the U.S. Army Research Office under grant No. W911NF-08-1-0449. A. M. Haimovich’s work was supported by the U.S. Air Force Office of Scientific Research under agreement No. FA9550-06-1-0026.

I. INTRODUCTION

Originally motivated by the recent advances in MIMO wireless communications [1], there has been many recent publications on MIMO radar [2]–[21]. In communications, MIMO systems combat the fading effects of the wireless (multi-path) channel with spatial diversity. Further, the scattering environment can be used by such systems to achieve spatial multiplexing.

In radar, complex targets consisting of several scatterers take the place of the multi-path channel. A target’s radar cross section (RCS), which determines the amount of returned power, varies greatly with the considered aspect angle. Those variations impair significantly the detection and estimation performance of conventional radar. MIMO radar systems observe a target simultaneously from different aspect angles resulting in spatial diversity. This diversity countervails the fluctuations in received power. In MIMO radar, one has M multiple transmit and N multiple receive antennas and all receive antennas pick up the signals from all transmit antennas which sets up MN paths. This allows for gains in performance which scale with MN . In [2] and [3], we explored the improvement MIMO radar can achieve in target detection and angle of arrival estimation relative to the performance of conventional (phased array) radar systems. The reader is referred to these publications for an extensive treatment of the target’s spatial RCS fluctuations and its effects in the MIMO radar context. In this paper, we analyze a MIMO radar approach, using orthogonal waveforms, for moving target detection.

In radar systems, it is common to exploit frequency shifts of the returned signals to distinguish between the returns of moving objects of interest and the ones due to the omnipresent clutter. Clutter, such as from forests or other vegetated surfaces, leads to only small frequency shifts, whereas the target’s radial movement results in larger frequency shifts. These differences have been employed in classical radar systems [22] to separate targets from clutter. Assuming that a target has a given absolute speed $|\mathbf{v}|$ and an angle Ω , the target’s velocity components in the x and y direction are given by

$$\begin{aligned} v_x &= |\mathbf{v}| \cos \Omega \\ v_y &= |\mathbf{v}| \sin \Omega. \end{aligned} \tag{1}$$

If a target is moving in a direction orthogonal to the direction of illumination from a conventional single antenna radar, whose single antenna is employed for both transmit and receive, this leads to a lack of Doppler shift in the received signal, impairing the ability of the radar to detect the target. In MIMO radar with widely dispersed antennas, we observe the target from several directions simultaneously, which overcomes this limitation of single antenna radar systems. We discussed these ideas and demonstrated these gains using analysis and simulations in [4], which is a preliminary conference version of the work presented here. Since that time, some nice complementary work has appeared in [23], which calls improvements of this type “geometry gains”. However, the problem, system, approach and assumptions considered in [23] are different from those considered in this paper which makes the two papers complementary. For example, in [23], a multistatic airborne radar, consisting of several phased array platforms, is considered for moving target detection. While we employ the MIMO radar architecture defined in [2], that exploits all the possible MN paths from the M available transmit antennas to the N available receive

antennas. As each platform only receives its own signal in the radar architecture studied in [23], all the possible MN paths are not exploited. Due to this, the radar architecture in [23] is therefore unable to fully exploit the diversity gains and the “geometry” gains available with our MIMO radar architecture. In this paper we show these gains, diversity and “geometry”, are distinct, which is not clear from the work in [23]. It should be noted that the idea called “geometry gain” has been discussed in other publications also.

In this paper, we provide analysis of a MIMO radar system with widely spaced multiple transmit and receive antennas, using orthogonal waveforms, for moving target detection in colored noise-plus-clutter. We illustrate the advantages of systems that use multiple transmit antennas over those using a single transmit antenna. We provide a comparison between conventional phased array radar and MIMO radar. We use receiver operating characteristic (ROC) curves of the test statistics to show the significant gains of the MIMO radar systems due to widely separating the antennas. We describe both centralized and distributed processing implementations of our MIMO radar architecture. We show that the centralized MIMO system performs better than the distributed one by comparing the cumulative distribution function (CDF) curves. We give analysis of the improvements due to spreading out the transmit antennas for MIMO radars. We also investigate constant false alarm rate (CFAR) detectors for the MIMO radar systems we consider.

II. SIGNAL MODELS

In this section, we develop two separate models, one for MIMO radar and one for conventional phased array radar.

A. MIMO Signal Model

We assume the target does not leave the given cell-under-test during K consecutive pulse transmissions. Furthermore, it is assumed that the M transmit elements employ pulse waveforms that maintain orthogonality under a variety of mutual delays and frequency shifts. This allows each of the N receive elements to separate the pulses transmitted by different transmit elements. Under the H_1 hypothesis (target present in the cell-under-test) and the H_0 hypothesis (target absent) respectively, the K consecutive signal samples at the l -th, $l = 1, \dots, N$ receiver due to the pulses from the k -th, $k = 1, \dots, M$ transmitter are given by the vector

$$\mathbf{r}_{k,l} = \begin{cases} \mathbf{c}_{k,l} + \mathbf{n}_{k,l} & H_0 \\ \alpha_{k,l} \cdot \mathbf{d}_{k,l}(v_x, v_y) + \mathbf{c}_{k,l} + \mathbf{n}_{k,l} & H_1. \end{cases} \quad (2)$$

The scalar $\alpha_{k,l}$ represents the unknown complex target reflectivity. We assume $\alpha_{k,l}$ does not vary during the K consecutive scans for any given k and l . Define

$$\mathbf{d}_{k,l}(f_{k,l}) = \begin{pmatrix} 1 \\ e^{j2\pi f_{k,l} T_{PRF}} \\ \vdots \\ e^{j2\pi f_{k,l} (K-1) T_{PRF}} \end{pmatrix}, \quad (3)$$

where T_{PRF} is the pulse repetition interval and $f_{k,l}$ denotes the observed Doppler shift at the l -th receiver due to the signal transmitted by the k -th transmitter. Note that

$$f_{k,l} = (\cos \theta_k^t + \cos \theta_l^r) \frac{f_c v_x}{c} + (\sin \theta_k^t + \sin \theta_l^r) \frac{f_c v_y}{c}, \quad (4)$$

where f_c is the carrier frequency and c the speed of light. The transmit and receive elements are located at angles θ_k^t and θ_l^r , respectively, when viewed from an origin located at the target. Figure 1 illustrates the geometry of this scenario. Now define

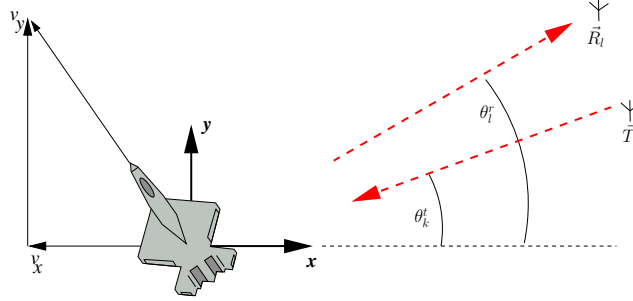


Fig. 1. Location of transmitter and receiver with respect to target and its movement.

$$\mathbf{d}_{k,l}(v_x, v_y) = \mathbf{d}_{k,l}(f_{k,l}) \Big|_{f_{k,l} = (\cos \theta_k^t + \cos \theta_l^r) \frac{f_c v_x}{c} + (\sin \theta_k^t + \sin \theta_l^r) \frac{f_c v_y}{c}}.$$

In (2), $\mathbf{c}_{k,l}$ represents the clutter echo and $\mathbf{n}_{k,l}$ the thermal noise at the receiver. We assume the clutter to be zero-mean complex Gaussian distributed with the following properties:

$$E\{\mathbf{c}_{k,l} \mathbf{c}_{k,l}^H\} = \mathbf{C}', \quad (5)$$

and

$$E\{\mathbf{c}_{k,l} \mathbf{c}_{k',l'}^H\} = \mathbf{0}_{K \times K}, \quad \forall k \neq k' \text{ or } l \neq l'. \quad (6)$$

The clutter correlation matrix \mathbf{C}' will be discussed in a later paragraph of this section. The thermal noise at the receive element is assumed to be zero-mean complex white Gaussian noise with the correlation matrix

$$E\{\mathbf{n}_{k,l} \mathbf{n}_{k,l}^H\} = \sigma_n^2 \mathbf{I}_{K \times K}.$$

The noise terms corresponding to different transmit-receive paths in (2) are assumed to be independent so that

$$E\{\mathbf{n}_{k,l} \mathbf{n}_{k',l'}^H\} = \mathbf{0}_{K \times K}, \quad \forall k \neq k' \text{ or } l \neq l'.$$

In the signal model just described, we ignore any different path losses between different transmitter-receiver pairs. Thus, we assume that all transmitters and receivers have roughly the same distance to the cell-under-test, but view this cell from different angles θ_k^t and θ_l^r .

B. Phased Array Signal Model

For comparison with conventional radars, we consider a radar system consisting of M transmit and N receive elements, co-located, jointly forming a linear array with small inter-element spacing. The transmit elements do not use different orthogonal pulse waveforms, but instead transmit the same waveform. The transmit elements steer a beam towards the direction ϕ_{tsteer} by imposing phase shifts on the transmit pulse. The phase shift at the k -th transmit element corresponds to $b_k(\phi_{\text{tsteer}}) = e^{j2\pi k \sin \phi_{\text{tsteer}} \Delta_t / \lambda}$, where Δ_t is the inter-element spacing on the transmit side and λ is the considered wavelength. The received K consecutive signal samples at the l -th, $l = 1, \dots, N$ array element are given by the vector

$$\mathbf{r}_l = \begin{cases} \sum_{k=1}^M \mathbf{c}_{k,l} b_k(\phi_{\text{tsteer}}) + \mathbf{n}_l & H_0 \\ \sum_{k=1}^M \left(a_l(\phi_r) \cdot \alpha \cdot \mathbf{d}(v_x, v_y) b_k^*(\phi_t) \right. \\ \quad \left. + \mathbf{c}_{k,l} \right) b_k(\phi_{\text{tsteer}}) + \mathbf{n}_l & H_1. \end{cases} \quad (7)$$

Here, the fading coefficient α is the same for all elements as they always view the same RCS aspect of the target. Further, the vector $\mathbf{d}(v_x, v_y)$ is the same across all elements as they have the same perspective with respect to the target's motion. The angle ϕ_t between the normal vector to the transmit array and the vector from the array to the target results in phase shifts of the impinging pulses given by $b_k(\phi_t) = e^{j2\pi k \sin \phi_t \Delta_t / \lambda}$. Furthermore, the angle ϕ_r between the normal vector to the receive array and the vector from the array to the target results in phase shifts across the receive array elements given by $a_l(\phi_r) = e^{j2\pi l \sin \phi_r \Delta_r / \lambda}$, where Δ_r is the inter-element spacing on the receive side. The noise components have the same properties as described for MIMO radar. The clutter properties will be discussed next.

C. Clutter Model

We employ a simple clutter model similar to the one used in [24]. Clutter exists everywhere, unlike a target, which has a limited extent. The clutter background is assumed spatially homogeneous, i.e., scatterers are governed by identical statistical distributions. Since the clutter echo received at each antenna is the result of a large sum of contributions from different clutter scatterers, it is asymptotically Gaussian. Such a model may apply to the returns from the forest, grassland or other homogeneous surfaces. Motivated by this, we adopt the usual assumptions for clutter. The clutter is also subject to internal motion such as due to wind. Thus, the received clutter echoes are complex Gaussian and the temporal clutter fluctuations are slow compared to the observation interval of K pulses.

A complete model of the clutter requires the specification of temporal and spatial correlation properties. The temporal correlation is described through the matrix \mathbf{C}' in (5). Since our processing is valid for any given \mathbf{C}' , we wait until the numerical results section to give the explicit form assumed there. In subsequent sections, we denote, for conciseness, the thermal noise and the clutter return as $\mathbf{x}_{k,l} = \mathbf{c}_{k,l} + \mathbf{n}_{k,l}$. The temporal correlation matrix of $\mathbf{x}_{k,l}$ is then $\mathbf{C} = E\{\mathbf{x}_{k,l} \mathbf{x}_{k,l}^H\} = \mathbf{C}' + \sigma_n^2 \mathbf{I}_{K \times K}$.

It is assumed, similar to (6), that the clutter returns corresponding to different transmit-receive paths are uncorrelated. This assumption is justified for widely spread antennas. For simplicity, we also employ this assumption for closely spaced antennas in the case of the conventional phased array radar. This is likely overly optimistic, thus overstating the true performance of the conventional phased array radar. Thus, we should expect even larger gains for MIMO radar in practice, over conventional phased array radar, compared to those shown here. We assume that for a given transmitter-receiver pair, the clutter temporal correlation is known or estimated a priori.

III. MOVING TARGET DETECTORS

Using the signal models defined in (2) and (7), we derive the detectors for the different schemes based upon the generalized likelihood ratio test (GLRT). We assume that in the cell-under-test, there is either a single target with a velocity vector $\mathbf{v} = [v_x, v_y]^T$ or no target at all.

A. Centralized MIMO Moving Target Detector

In standard MIMO radar, we assume centralized processing such that all received signals corresponding to the MN transmit-receive paths in (2) are transmitted to a central station for joint processing. Stacking the MN received vectors $\mathbf{r}_{k,l}$ in one vector $\mathbf{r} = [\mathbf{r}_{1,1}^T, \dots, \mathbf{r}_{M,N}^T]^T$ and the MN target coefficients $\alpha_{k,l}$ in the vector $\boldsymbol{\alpha} = [\alpha_{1,1}, \dots, \alpha_{M,N}]^T$, we can write the joint probability density function of the received vectors conditioned on the hypotheses and parameters as

$$f(\mathbf{r}|\boldsymbol{\alpha}, v_x, v_y, H_1) = \prod_{k=1}^M \prod_{l=1}^N \frac{1}{\pi^K \sqrt{\det \{\mathbf{C}\}}} \cdot e^{-\left(\mathbf{r}_{k,l} - \alpha_{k,l} \mathbf{d}_{k,l}(v_x, v_y)\right)^H \mathbf{C}^{-1} \left(\mathbf{r}_{k,l} - \alpha_{k,l} \mathbf{d}_{k,l}(v_x, v_y)\right)} \quad (8)$$

and

$$f(\mathbf{r}|H_0) = \prod_{k=1}^M \prod_{l=1}^N \frac{1}{\pi^K \sqrt{\det \{\mathbf{C}\}}} e^{-\mathbf{r}_{k,l}^H \mathbf{C}^{-1} \mathbf{r}_{k,l}}, \quad (9)$$

where we used $\mathbf{C} = \mathbf{C}' + \sigma_n^2 \mathbf{I}_{K \times K}$. The GLRT is then defined [25] as

$$\hat{\xi} = \ln \left(\frac{\max_{\boldsymbol{\alpha}, v_x, v_y} f(\mathbf{r}|\boldsymbol{\alpha}, v_x, v_y, H_1)}{f(\mathbf{r}|H_0)} \right) \underset{H_0}{\overset{H_1}{\geq}} \hat{\gamma}. \quad (10)$$

We note now that maximizing $f(\mathbf{r}|\boldsymbol{\alpha}, v_x, v_y, H_1)$ with respect to $\boldsymbol{\alpha}, v_x$ and v_y is equivalent to minimizing

$$\sum_{k=1}^M \sum_{l=1}^N \left(\mathbf{r}_{k,l} - \alpha_{k,l} \mathbf{d}_{k,l}(v_x, v_y)\right)^H \mathbf{C}^{-1} \left(\mathbf{r}_{k,l} - \alpha_{k,l} \mathbf{d}_{k,l}(v_x, v_y)\right), \quad (11)$$

which in turn is equivalent to maximizing

$$\sum_{k=1}^M \sum_{l=1}^N 2\Re\{\alpha_{k,l}^* \mathbf{d}_{k,l}^H(v_x, v_y) \mathbf{C}^{-1} \mathbf{r}_{k,l}\} - |\alpha_{k,l}|^2 \mathbf{d}_{k,l}^H(v_x, v_y) \mathbf{C}^{-1} \mathbf{d}_{k,l}(v_x, v_y). \quad (12)$$

Furthermore, the expression (12) is maximized for any given pair v_x and v_y by

$$\alpha_{k,l} = \frac{\mathbf{d}_{k,l}^H(v_x, v_y) \mathbf{C}^{-1} \mathbf{r}_{k,l}}{\mathbf{d}_{k,l}^H(v_x, v_y) \mathbf{C}^{-1} \mathbf{d}_{k,l}(v_x, v_y)}. \quad (13)$$

Using (8) in (10) results in the following decision rule:

$$\xi = \max_{v_x, v_y} \sum_{k=1}^M \sum_{l=1}^N \frac{|\mathbf{d}_{k,l}^H(v_x, v_y) \mathbf{C}^{-1} \mathbf{r}_{k,l}|^2}{\mathbf{d}_{k,l}^H(v_x, v_y) \mathbf{C}^{-1} \mathbf{d}_{k,l}(v_x, v_y)} \underset{H_0}{\overset{H_1}{\geq}} \gamma. \quad (14)$$

We emphasize that the centralized MIMO moving target detector employs a joint estimate of the true velocity vector $\mathbf{v} = (v_x, v_y)$ formed using all elements of \mathbf{r} . In the next section, we discuss the implications of this joint estimate when compared to local velocity estimates determined at each receive antenna.

B. Distributed MIMO Moving Target Detector

When distributed processing is adopted in MIMO radar, the system complexity is dramatically reduced. Here we investigate a simple type of distributed processing, and compare its complexity and performance with those of centralized processing. In this case, each receive station (receive antenna) processes its received signal autonomously and transmits a local decision to a fusion center.

We implement a distributed MIMO detector utilizing soft decisions as described by the following test and global test statistic

$$\xi = \sum_{k=1}^M \sum_{l=1}^N \max_{f_{k,l}} \frac{|\mathbf{d}_{k,l}^H(f_{k,l}) \mathbf{C}^{-1} \mathbf{r}_{k,l}|^2}{\mathbf{d}_{k,l}^H(f_{k,l}) \mathbf{C}^{-1} \mathbf{d}_{k,l}(f_{k,l})} \underset{H_0}{\overset{H_1}{\geq}} \gamma. \quad (15)$$

This expression implies that the l -th receive station estimates the Doppler shift $f_{k,l}$ based on the signal transmitted by the k -th transmit station only. The soft decisions are transferred to the fusion center that sums all the soft decisions to compute the final test statistic. Thus, instead of transmitting K samples per test for each transmitter-receiver pair to the central station, as in the centralized MIMO case, only one sample is sent to the fusion center. It can be argued that binary or multi-bit local decisions, as described in [18], [26]–[29], are a form of quantization of those samples. Following the common observation that the fusion of soft decisions outperforms the fusion of hard decisions, we can infer that a detector based on (15) performs at least as good as a detector based on binary or multi-bit decisions.

For distributed MIMO, as per (15), one needs to perform a one dimensional search to find the Doppler shift $f_{k,l}$ that corresponds to each of the MN paths. Let us denote the complexity of this search as η , which stands for the average number of computations needed to perform the one dimensional search. At each receive antenna, one has to perform the search M times for each transmitted signal, so the complexity at each receiver is $M\eta$. The total complexity at all N receive antenna is $MN\eta$ for the distributed MIMO system. For the centralized MIMO system, one needs to perform a two dimensional search, as per (14), to find the two dimensional vector (v_x, v_y) , and the complexity would be on the order of η^2 . If M and N are reasonably small, the complexity of the distributed

MIMO system will be lower. Of course, since the Doppler shift estimate, on which the GLRT test statistic is based, is produced for each path individually and independently while physically all the Doppler shifts correspond to a common target, the performance of the distributed system will be inferior.

C. Phased Array Moving Target Detector

A conventional phased array radar will steer a transmit beam and a receive beam towards the cell-under-test. The beamformer on the transmit side is already incorporated in the signal model (7). The beamformer on the receive side sums the N received signal vectors from (7) into a single received vector \mathbf{r}

$$\mathbf{r} = \sum_{l=1}^N a_l^*(\phi_{\text{rsteer}}) \mathbf{r}_l, \quad (16)$$

where ϕ_{rsteer} is defined similar to ϕ_r .

Our model can be shown to be consistent with the model in [22]. In particular, we can show our SINR scales with N in the same way as does the model in [22].

The moving target detection procedure is based on the single $K \times 1$ vector \mathbf{r} . Assume that the steering angle ϕ_{rsteer} matches the angle of arrival ϕ_r . Following the same derivation as in Section III-A, the test statistic is derived as

$$\xi = \max_{f_d} \frac{|\mathbf{d}^H(f_d) \mathbf{C}^{-1} \mathbf{r}|^2}{\mathbf{d}^H(f_d) \mathbf{C}^{-1} \mathbf{d}(f_d)} \underset{H_0}{\overset{H_1}{\geq}} \gamma. \quad (17)$$

We note again that the conventional phased array radar observes only one Doppler shift f_d resulting from the target's radial velocity. Accordingly, the GLRT test statistic is based on an estimate of this frequency shift, as (17) indicates.

D. Adaptive MIMO Moving Target Detector

All the decision statistics previously described have been derived under the assumption of known noise-plus-clutter (called interference in the sequel) temporal correlation matrix \mathbf{C} . However, in reality this matrix might be unknown. Moreover, different transmitter-receiver pairs in the centralized or decentralized MIMO system might be subject to different interference levels or characteristics, and thus have different interference matrices. Accordingly, we use $\mathbf{C}_{k,l}$ to denote the interference matrix for the path between of the k -th transmitter and the l -th receiver.

It is possible to convert all of the previously described detectors to adaptive detectors that maintain a constant false alarm rate (CFAR) [30], [31]. This is accomplished by replacing the true clutter covariance matrix by its estimate

$$\hat{\mathbf{C}}_{k,l} = \frac{1}{L} \sum_{i=1}^L \mathbf{r}_{k,l}(i) \mathbf{r}_{k,l}(i)^H \quad (18)$$

based on $L > K$ “secondary” data vectors, $\mathbf{r}_{k,l}(i)$. We note that the $\mathbf{r}_{k,l}(i)$ are measured in adjacent range cells, for which target absence is assumed. Refer to [32] and [30] for details. The adaptive centralized MIMO test statistic is then given as

$$\xi = \max_{v_x, v_y} \sum_{k=1}^M \sum_{l=1}^N \frac{|\mathbf{d}_{k,l}^H(v_x, v_y) \hat{\mathbf{C}}_{k,l}^{-1} \mathbf{r}_{k,l}|^2}{\mathbf{d}_{k,l}^H(v_x, v_y) \hat{\mathbf{C}}_{k,l}^{-1} \mathbf{d}_{k,l}(v_x, v_y)} \underset{H_0}{\overset{H_1}{\geq}} \gamma. \quad (19)$$

In Appendix I, it is shown that this test statistic is indeed subject to CFAR behavior. The same result can easily be extrapolated to the adaptive distributed MIMO and phased array cases. In this context, it is noted that the clutter is assumed to have the same statistical characteristics for all transmitter-receiver pairs in the phased array system.

In Section IV-D, the CFAR property of the test statistic (19) is demonstrated with numerical results, and the performances of the MIMO and phased array system in adaptive mode are compared.

IV. SIMULATION RESULTS AND INFERENCES

In this section, we discuss simulation results and compare the performance of the different systems and setups. First, we describe the choice of the clutter covariance matrix \mathbf{C}' . Assuming internal motion of the clutter scatterers such as due to wind affecting a forest or grassland, the temporal correlation of such clutter can be described by its power spectral density (PSD) (for example, [22] or [33])

$$S_{cc}(f) = \frac{P_{cc}\lambda}{\sqrt{2\pi}2\sigma_v} e^{-\frac{f^2\lambda^2}{8\sigma_v^2}}, \quad (20)$$

where P_{cc} is the clutter power, λ the wavelength, and σ_v the RMS of clutter velocity. This relates to a continuous autocorrelation function (ACF) of

$$\varphi_{cc}(\tau) = \int_{-\infty}^{\infty} \frac{P_{cc}\lambda}{\sqrt{2\pi}2\sigma_v} e^{-\frac{f^2\lambda^2}{8\sigma_v^2}} e^{j2\pi f\tau} df \quad (21)$$

$$= P_{cc} e^{-\pi^2\tau^2 8\frac{\sigma_v^2}{\lambda^2}}. \quad (22)$$

Sampling this ACF at $\tau = kT_{PRF}$, $k = 0, \dots, K-1$, we find the correlation coefficients $\rho_{cc}(k)$ of the K consecutive samples, i.e., $\rho_{cc}(k) = \varphi_{cc}(kT_{PRF})$. The clutter temporal correlation matrix is then given as

$$\mathbf{C}' = \begin{pmatrix} \rho_{cc}(0) & \rho_{cc}(1) & \cdots & \rho_{cc}(K-1) \\ \rho_{cc}(1) & \rho_{cc}(0) & & \vdots \\ \vdots & & \ddots & \rho_{cc}(1) \\ \rho_{cc}(K-1) & \cdots & \rho_{cc}(1) & \rho_{cc}(0) \end{pmatrix}. \quad (23)$$

In the simulations, we assume the carrier frequency $f_c = 1\text{GHz}$, the number of time samples $K = 10$, and the RMS of clutter velocity $\sigma_v = 1.25\text{m/s}$. The search procedures to obtain the GLRT statistics for different systems are performed over a certain velocity range corresponding to the unambiguous velocities determined by the chosen PRF.

A. Receiver Operating Characteristics

Here, we compare the different radar systems according to their receiver operating characteristics (ROC). Assume the pulse repetition frequency is 500Hz, the clutter-to-noise ratio is 40dB, and each radar system has 2 transmitters and 2 receivers, where the transmitters are located at $\{\theta_k^t\}_{k=1}^2 = \{0^\circ, 65^\circ\}$ and the receivers are located at $\{\theta_l^r\}_{l=1}^2 = \{-30^\circ, 40^\circ\}$. Consider a target with $\alpha_{k,l} = \alpha = \text{constant}$ (nonrandom) in (2), where $k = 1, 2$ and $l = 1, 2$. Further assume the target moves with random direction and velocity magnitude of 68km/h. Choosing $\alpha_{k,l} = \alpha = \text{constant}$ allows us to isolate the “geometry gains” from the diversity gains by essentially turning off the diversity gains by eliminating target fluctuations. Figure 2 shows the ROCs of the centralized MIMO (CMIMO), distributed MIMO (DMIMO), and conventional phased array (conv.) radar systems for different target-to-clutter (tc) ratios. It is observed that the ROC curves for the centralized MIMO are on top of each other and the corresponding detection probabilities are close to 1, which shows the performance of the centralized MIMO systems is quite good in all these cases. Due to the “geometry gains”, the MIMO radars outperform the conventional phased array radars, which observe the target only from one aspect. The conventional phased array radar is limited to observe the target from only one viewing angle per array, which can lead to poor performance, in comparison with MIMO radar, with random target direction. Note that the effect of random target direction is similar to that of target RCS fluctuation. The reason is that the conventional radars perform well only for certain target directions that are consistent with their viewing angles. For these target directions, the effect is like a large RCS return. For other target directions, the effect is like a small RCS return.

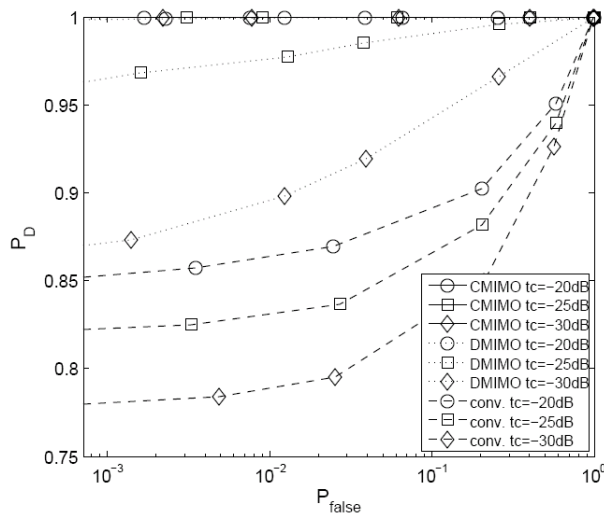


Fig. 2. ROCs for a 68km/h target with random direction and $\alpha_{k,l} = \alpha = \text{constant}$ (PRF=500Hz, CNR=40dB).

Figure 3 repeats the experiment in Figure 2, while accounting for the target’s RCS fluctuations. In this case, we select $\alpha_{k,l}$, $k = 1, \dots, M$ and $l = 1, \dots, N$, in (2) as a set of complex Gaussian random variables. MIMO radars again outperform the conventional phased array radars. However, this time the improvement is due to both

“geometry” and spatial diversity gains. The spatial diversity gains reduce the effects of the RCS fluctuations over different transmitter-receiver paths.

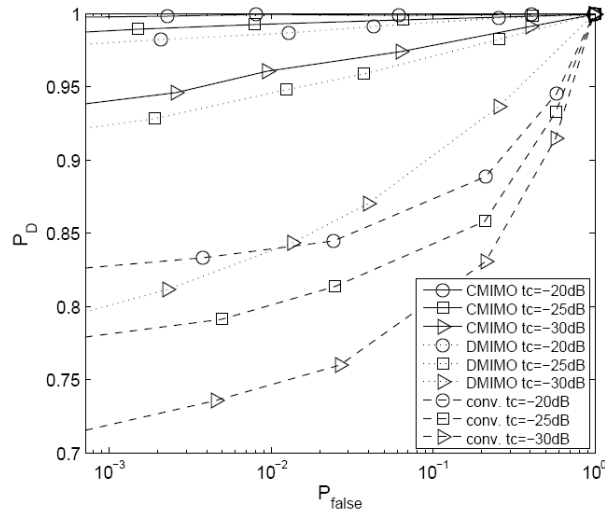


Fig. 3. ROCs for a 68km/h target with random direction and a set of complex Gaussian $\alpha_{k,l}$ (PRF=500Hz, CNR=40dB).

Taken together, Figures 2 and 3 demonstrate two separate gains for MIMO radar, when compared to the conventional phased array radar. MIMO radar has the ability to view the moving target from different directions, while the phased array views only from one direction per array. Thus, if the target moves perpendicular to the phased array viewing direction, performance is degraded. This is called “geometry gain” here [23]. The other gain is the diversity gain [2]. The first gain leads to the improvements in Figure 2 while the two gains together lead to the much larger gains in Figure 3.

For completeness, we remind the reader that, as demonstrated in [2], MIMO radar is not always better than the conventional phased array approach. As described in [2], MIMO radar is better for cases with sufficiently high SNR. At very low SNR, the conventional phased array approach is better. The interested reader is referred to [2] for performance curves, analysis, and discussion which is not repeated here in the interest of brevity. Thus if we were to significantly decrease the signal strength in the cases studied here we would eventually encounter this phenomenon. However, since we consider moving targets in this paper, as opposed to [2], we would find that MIMO radar is better for even lower signal strengths than predicted in [2]. The reason is the geometry-based MIMO radar gains over the conventional phased array approach which come in addition to the diversity gains studied in [2] when one employs widely separated antennas. Extensive simulation results, which are very similar in nature to those given in [2], have verified this.

B. Comparing Centralized and Distributed MIMO Radars

In this section, we give more insight into the centralized and distributed MIMO detectors by comparing the cumulative distribution functions (CDF) of their test statistics with a focus on the “geometry gains” only. Assume

the pulse repetition frequency is 2KHz, the clutter-to-noise ratio is 30dB, a single transmitter is located at $\theta_1^t = 0^\circ$, and the locations of the receivers are as follows: when $N = 1$, $\theta_1^r = 0^\circ$; when $N = 4$, $\{\theta_l^r\}_{l=1}^4 = \{-39^\circ, -13^\circ, 13^\circ, 39^\circ\}$; when $N = 8$, $\{\theta_l^r\}_{l=1}^8 = \{-39^\circ, -26^\circ, -13^\circ, 0^\circ, 13^\circ, 26^\circ, 39^\circ, 51^\circ\}$. Assume the target-to-clutter ratio is 0dB. Figure 4 shows the CDF of the test statistics for centralized and distributed MIMO radars under hypothesis H_1 , where a target with $\alpha_{k,l} = \alpha = \text{constant}$ and absolute velocity 300km/h is present. Note that for this choice of target-to-clutter ratio, the test statistics for both systems (as defined in (14) and (15)), follow a similar distribution. Figure 5 shows the CDF of the test statistics for centralized and distributed MIMO radars under hypothesis H_0 , where the target is absent and the received signal contains only noise-plus-clutter. These plots show that for a given CDF value $F(\xi|H_0)$, the test statistic ξ_{H_0} for centralized MIMO radar is smaller than the one for distributed MIMO radar.

Recall that for a threshold γ , the detection probability is $P_d = 1 - F(\gamma|H_1)$ and the false alarm probability is $P_{fa} = 1 - F(\gamma|H_0)$. Comparing the CDF curves in Figure 4 and Figure 5, we find that to get the same detection probability P_d , the centralized MIMO detector and the distributed MIMO detector need a threshold of similar size, while given a threshold of similar size the former has lower P_{fa} . This explains the gains we saw in Figures 2 and 3 already for the centralized MIMO detector in terms of the statistics of the tests involved. Unlike the distributed detector which performs a one-dimensional search for each transmit-receive path, the centralized detector searches over a two-dimensional space jointly based on all available samples. The joint maximization approach in centralized MIMO radar imposes more restrictions on the test statistic, and thus effectively reduces the chances for false alarms. This is why the centralized MIMO radar outperforms the distributed MIMO radar. Keep in mind that the two-dimensional search for centralized MIMO radar demands higher computational complexity.

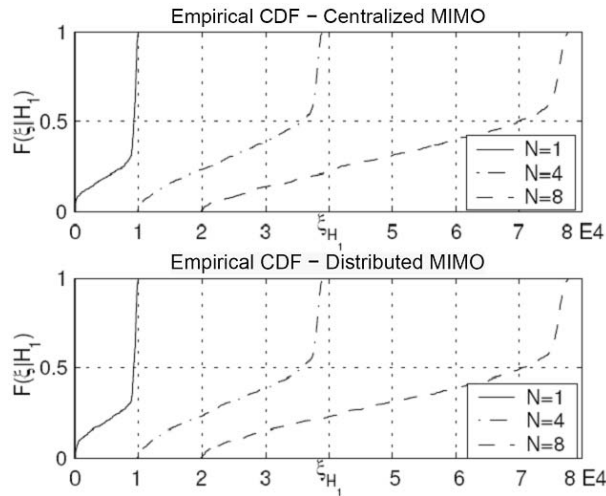


Fig. 4. CDFs of ξ given H_1 for different numbers of receiver antennas.

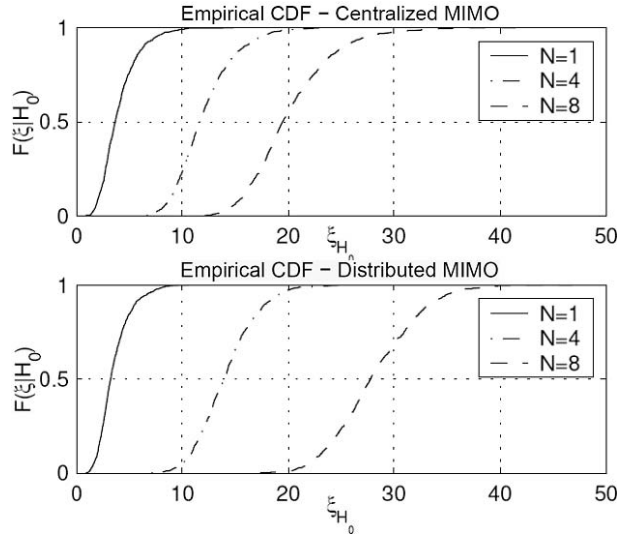


Fig. 5. CDFs of ξ given H_0 for different numbers of receiver antennas.

C. Distributed Transmitter Elements

The target Doppler shift $f_{k,l}$ caused by the k, l -th transmit-receive path can be represented as [34]

$$f_{k,l} = \frac{2f_c|\mathbf{v}|}{c} \cos(\phi_{k,l}^{bs}) \cos\left(\frac{\theta_k^t - \theta_l^r}{2}\right), \quad (24)$$

where $|\mathbf{v}|$ denotes the target absolute velocity. The transmitter and receiver have aspect angles θ_k^t and θ_l^r referenced to the horizontal axis, as shown in Figure 6. The angle $\phi_{k,l}^{bs}$ is measured between the target velocity vector and the bisector of the transmitter-target-receiver angle. From (24), for a given absolute target velocity, the magnitude

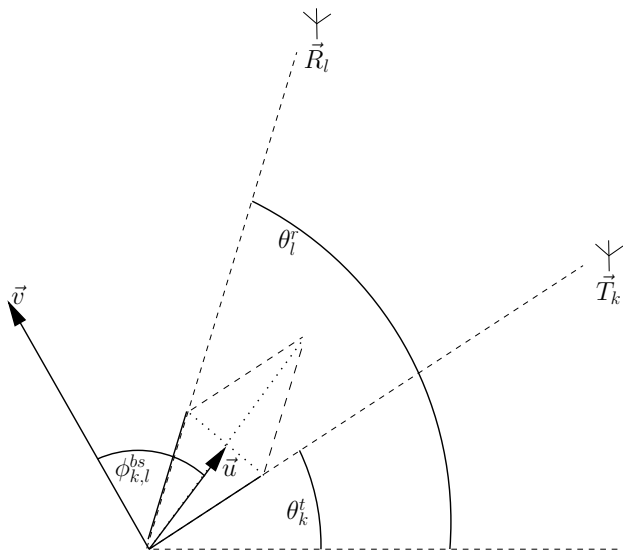


Fig. 6. Illustration of the bistatic bisector and its impact.

of the Doppler shift $f_{k,l}$ is determined by $\phi_{k,l}^{bs}$ and $(\theta_k^t - \theta_l^r)$. On one hand, widely-dispersed antennas in MIMO radar ensure that some antenna will yield $\cos(\phi_{k,l}^{bs}) \approx 1$. On the other hand, to get large Doppler shifts, the difference between the transmitter and the receiver aspects should be kept small. The validity of this argument is demonstrated by comparing a 1×8 and a 2×4 centralized MIMO radar. Assume the pulse repetition frequency is 2KHz and the clutter-to-noise ratio is 30dB. The element locations of the 1×8 system are $\theta_1^t = 45^\circ$ and $\{\theta_l^r\}_{l=1}^8 = \{0^\circ, 13^\circ, 26^\circ, 38^\circ, 50^\circ, 62^\circ, 75^\circ, 90^\circ\}$. The 2×4 system consists of transmitter and receiver elements located at $\{\theta_k^t\}_{k=1}^2 = \{5^\circ, 85^\circ\}$ and $\{\theta_l^r\}_{l=1}^4 = \{0^\circ, 30^\circ, 60^\circ, 90^\circ\}$. The total transmit energy of the 2×4 system is twice that of the 1×8 system. According to the analysis presented in [2], these two systems should perform identically in a non-moving target situation, since they have the same number of “diversity branches” (i.e., $N \cdot M = 8$) and emit the same power per transmitter. However, Figure 7 shows that the system with two transmitters outperforms the single transmitter system under the moving target model considered in this paper. This is an interesting observation, as it contrasts possible inferences from the analysis found for stationary targets in [2]. Further, noting that the 1×8 system has a total of 9 transmit or receive stations whereas the 2×4 system has only 6 stations, the preference towards systems with multiple transmitter elements may be strengthened by an economical argument.

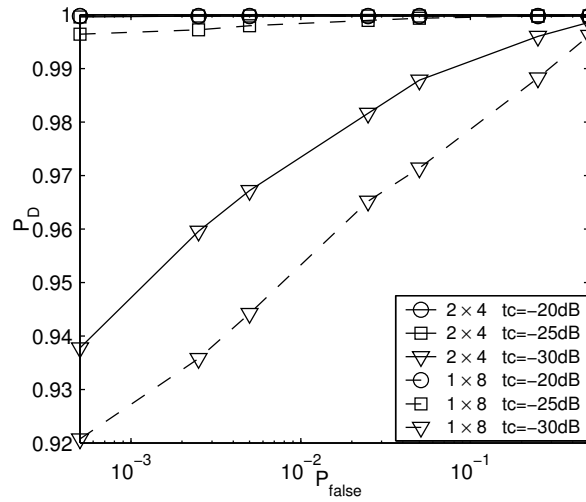


Fig. 7. ROCs for a 300km/h target with random direction for a 1×8 and 2×4 system (PRF=2KHz, CNR=30dB).

D. CFAR Properties of the Test Statistics

In this section, we discuss 1×4 and 1×8 centralized MIMO and phased array systems. Assume the pulse repetition frequency is 2KHz and the clutter-to-noise ratio is 30dB. Figure 8 shows the empirical CDFs of the adaptive centralized MIMO test statistic, (19), under H_0 for a 1×4 system and different numbers of secondary vectors, L . The transmit and receive elements have the same positions as in Section IV-B.

The solid curve is the CDF for the known clutter covariance matrix. The dashed curves reflect the empirical CDF of the test statistic ξ under H_0 for $L = 160$, and the dotted ones denote $L = 40$. For each L , two scenarios are

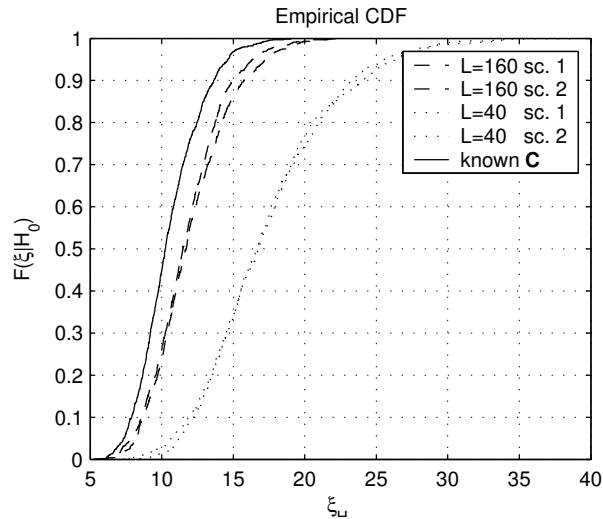


Fig. 8. CDFs for a CFAR 1×4 system with different amounts of secondary samples.

considered:

- Scenario 1 (sc. 1): The clutter covariance matrix is the same for all receive elements, and has the previously described form (see (23), assuming the pulse repetition frequency is 2KHz and the clutter-to-noise ratio is 30dB).
- Scenario 2 (sc. 2): Two of the four receive elements observe clutter returns with the same covariance matrix as before. For the other two, the clutter-to-noise ratio is reduced by 20 dB and the complete interference power raised by 6 dB.

In either case, secondary data vectors are used to estimate the covariance matrix, as in (18). The almost identical empirical CDFs for the two scenarios illustrate that the adaptive test statistic has a distribution that is independent of the underlying clutter characteristic and, therefore, can be used to achieve at least approximate CFAR properties. However, the number of secondary vectors used in the estimate of the covariance matrix has an impact on the test statistic distribution. For small values of L the variance of the test statistic under H_0 increases. This leads to a reduced P_d , and is a well observed fact for CFAR detection, [30].

Figure 9 shows the ROCs for 1×8 MIMO and phased array radar systems for CFAR detection. Here $L = 200$ secondary data vectors are used. A target with a speed of $|\mathbf{v}| = 300\text{km/h}$ is considered for H_1 . In this case, though the performance of both centralized MIMO radar and phased array radar is slightly impaired from not having exact knowledge of \mathbf{C} , the centralized MIMO system still outperforms the phased array system.

V. CONCLUSIONS

In this paper, we analyzed the performance of MIMO radar for a moving target detection problem. We developed signal models for the MIMO radar and a phased array radar to compare their performance in detecting moving

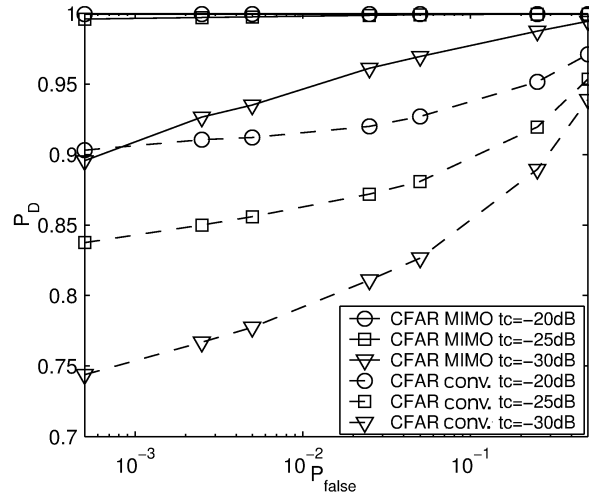


Fig. 9. ROCs for a 300km/h target with random direction for a phased array and 1×8 MIMO CFAR system, $L = 200$ (PRF=2KHz, CNR=30dB).

targets in colored Gaussian noise-plus-clutter. We derived GLRT moving target detectors for centralized MIMO, distributed MIMO and a phased array radar system, respectively. We showed that the MIMO radar approach obtains a probability of detection for moving targets with small radial velocities that can not be obtained by the conventional phased array radar. We quantified the degradation from employing distributed MIMO radar in place of the more computationally demanding centralized MIMO radar implementation. The importance of proper antenna placement was discussed, and an adaptive version of the MIMO radar moving target detector was proposed. This adaptive detector was shown to provide constant false alarm probability for homogeneous clutter.

APPENDIX I

CFAR PROPERTIES OF THE MIMO MTD

In this appendix, the CFAR properties of the MIMO moving target detector are explored. The way this is done is similar to [31]. The adaptive MIMO moving target detector decision statistic has the form

$$\xi = \max_{v_x, v_y} \sum_{k=1}^M \sum_{l=1}^N \frac{\left| \mathbf{d}_{k,l}^H(v_x, v_y) \hat{\mathbf{C}}_{k,l}^{-1} \mathbf{r}_{k,l} \right|^2}{\mathbf{d}_{k,l}^H(v_x, v_y) \hat{\mathbf{C}}_{k,l}^{-1} \mathbf{d}_{k,l}(v_x, v_y)} \underset{H_0}{\overset{H_1}{\geq}} \gamma, \quad (25)$$

where $\hat{\mathbf{C}}_{k,l}$ is an estimate of the covariance matrix of the clutter observed by the k, l transmitter-receiver pair based on L secondary sample vectors. We focus now on a single term of the sum in the test statistic. By substituting $\mathbf{d}_{k,l}(v_x, v_y)$ with $\mathbf{C}_{k,l}^{1/2} \mathbf{d}'_{k,l}(v_x, v_y)$ and $\mathbf{r}_{k,l}$ with $\mathbf{C}_{k,l}^{1/2} \mathbf{r}'_{k,l}$ each term is given as

$$\frac{\left| \mathbf{d}'_{k,l}{}^H(v_x, v_y) \mathbf{C}_{k,l}^{1/2} \hat{\mathbf{C}}_{k,l}^{-1} \mathbf{C}_{k,l}^{1/2} \mathbf{r}'_{k,l} \right|^2}{\mathbf{d}'_{k,l}{}^H(v_x, v_y) \mathbf{C}_{k,l}^{1/2} \hat{\mathbf{C}}_{k,l}^{-1} \mathbf{C}_{k,l}^{1/2} \mathbf{d}'_{k,l}(v_x, v_y)} = \frac{\left| \mathbf{d}'_{k,l}{}^H(v_x, v_y) \hat{\mathbf{C}}_{k,l}^{-1} \mathbf{r}'_{k,l} \right|^2}{\mathbf{d}'_{k,l}{}^H(v_x, v_y) \hat{\mathbf{C}}_{k,l}^{-1} \mathbf{d}'_{k,l}(v_x, v_y)}. \quad (26)$$

It is noted that $\hat{\mathbf{C}}'_{k,l} = \mathbf{C}_{k,l}^{-1/2} \hat{\mathbf{C}}_{k,l} \mathbf{C}_{k,l}^{-1/2}$ follows a complex Wishart distribution, $\mathcal{CW}(L, K, \mathbf{I})$ with mean \mathbf{I} and thus its distribution is independent of the actual clutter covariance $\mathbf{C}_{k,l}$. Further, $\mathbf{r}'_{k,l}$ under H_0 is a complex Gaussian vector with zero mean and covariance matrix \mathbf{I} , $\mathcal{CN}(\mathbf{0}, \mathbf{I})$. Moreover, for any $\mathbf{d}'_{k,l}(v_x, v_y)$ a unitary matrix \mathbf{U} can be found that rotates it onto the first elementary vector, $c\mathbf{e} = \mathbf{U}^H \mathbf{d}'_{k,l}(v_x, v_y)$. With $\mathbf{r}''_{k,l} = \mathbf{U}^H \mathbf{r}'_{k,l}$ and $\hat{\mathbf{C}}''_{k,l} = \mathbf{U}^H \hat{\mathbf{C}}'_{k,l} \mathbf{U}$ expression (26) becomes

$$\frac{\left| c\mathbf{e}^H(v_x, v_y) \hat{\mathbf{C}}''_{k,l}{}^{-1} \mathbf{r}''_{k,l} \right|^2}{|c|^2 \mathbf{e}^H \hat{\mathbf{C}}''_{k,l}{}^{-1} \mathbf{e}} = \frac{\left| \mathbf{e}^H(v_x, v_y) \hat{\mathbf{C}}_{k,l}{}^{-1} \mathbf{r}'_{k,l} \right|^2}{\mathbf{e}^H \hat{\mathbf{C}}_{k,l}{}^{-1} \mathbf{e}}. \quad (27)$$

Note that $\mathbf{r}''_{k,l}$ and $\hat{\mathbf{C}}''_{k,l}$ follow the same distributions as $\mathbf{r}'_{k,l}$ and $\hat{\mathbf{C}}'_{k,l}$, respectively, and are thus independent of the actual $\mathbf{C}_{k,l}$. Therefore, the term in expression (27) is for any v_x, v_y and any k, l independent of the respective $\mathbf{C}_{k,l}$. Accordingly, the decision statistic under H_0 in (25) leads to constant false alarm rate.

REFERENCES

- [1] Bölcskei, H., and A. J. Paulraj, *The Communications Handbook*, 2nd ed. CRC Press, 2002, ch. Multiple-input multiple-output (MIMO) wireless systems, pp. 90.1 – 90.14.
- [2] E. Fishler, A. M. Haimovich, R. Blum, L. Cimini, D. Chizhik, and R. Valenzuela, “Spatial diversity in radars - models and detection performance,” *IEEE Trans. on Signal Processing*, vol. 54, no. 3, pp. 823–838, March 2006.
- [3] N. Lehman, E. Fishler, A. M. Haimovich, R. S. Blum, L. Cimini, and R. Valenzuela, “Evaluation of Transmit Diversity in MIMO-radar Direction Finding,” *IEEE Trans. on Signal Processing*, vol. 55, no. 5, pp. 2215–2225, May 2007.
- [4] N. Lehmann, A. M. Haimovich, R. S. Blum, and L. Cimini, “MIMO-Radar application to moving target detection in homogeneous clutter,” *14th Annual Workshop on Adaptive Sensor Array Processing*, June 2006.
- [5] P. F. Sannmartino, C. J. Baker, and H. D. Griffiths, “Target model effects on mimo radar performance,” *IEEE International Conference on Acoustics, Speech and Signal Processing*, vol. 5, pp. 1129–1132, May 2006.
- [6] D. W. Bliss and K. W. Forsythe, “Multiple-input multiple-output (mimo) radar and imaging: Degrees of freedom and resolution,” in *Proc. 37th Asilomar Conf. Singal, System and Computers*, pp. 54–59, November 2003.
- [7] J. Li, P. Stoica, L. Xu, and W. Roberts, “On parameter identifiability of mimo radar,” *IEEE Signal Processing Letters*, vol. 14, no. 12, pp. 968–971, December 2007.
- [8] J. Li and P. Stoica, “Mimo radar with colocated antennas: Review of some recent work,” *IEEE Signal Processing Magazine*, vol. 24, no. 5, pp. 106–114, September 2007.
- [9] D. R. Fuhrmann and G. S. Antonio, “Transmit beamforming for mimo radar systems using partial signal correlation,” in *Proc. 38th Asilomar Conf. Singal, System and Computers*, pp. 295–299, November 2004.
- [10] J. Li, L. Xu, P. Stoica, D. Bliss, and K. Forsythe, “Range compression and waveform optimization for mimo radar - a cramer-rao bound based study,” *IEEE Transactions on Signal Processing*, vol. 56, no. 1, pp. 218–232, January 2008.
- [11] P. Stoica, J. Li, and Y. Xie, “On probing signal design for mimo radar,” *IEEE Transactions on Signal Processing*, vol. 55, no. 8, pp. 4151–4161, August 2007.
- [12] P. Stoica, J. Li, X. Zhu, and B. Guo, “Waveform synthesis for diversity-based transmit beampattern design,” *the 14th IEEE Workshop on Statistical Signal Processing (invited), Madison, Wisconsin*, August 2007.
- [13] F. C. Robey, S. Coutts, D. Werikle, C. Mcharg, and K. Cuomo, “Mimo radar theory and eperimental results,” in *Proc. 38th Asilomar Conf. Singal, System and Computers*, pp. 300–304, November 2004.
- [14] P. F. Sannmartino, C. J. Baker, and H. D. Griffiths, “Adaptive mimo radar systems in clutter,” *IEEE Radar Conference*, pp. 276–281, April 2007.
- [15] L. Xu, J. Li, and P. Stoica, “Adaptive techniques for mimo radar,” *14th IEEE Workshop Sensor Array and Multi-channel Processing*, July 2006.

- [16] E. D'Addio and A. Farina, "Overview of detection theory in multistatic radar," *IEE Proc., Part F*, vol. 133, no. 7, pp. 613–623, December 1986.
- [17] I. Papoutsis, C. Baker, and H. Griffiths, "Fundamental Performance Limitations of Radar Networks," in *Proc. of the 1st EMRS DTC Technincal Conference, Edingburgh*, 2004.
- [18] V. S. Chernyak, *Fundamentals of Multisite Radar Systems*, 1st ed. Gordon and Breach Science Publishers, 1998.
- [19] F. Gini, A. Farina, and M. Greco, "Selected list of references on radar signal processing," *IEEE Transactions on Aerospace and Electronic Systems*, vol. 37, no. 1, pp. 329–259, January 2001.
- [20] A. R. Elias-Fuste and A. P. Broquetas-Ibars, "Constant False Alarm Rate for a Radar Data Fusion Center with N Parallel Distributed Cell Averaging Receivers," *IEEE International Radar Conference*, pp. 507–510, May 1990.
- [21] W. Liu, Y. Lu, and J. S. Fu, "A novel method for CFAR data fusion," *Neural Networks for Signal Processing, IEEE Signal Processing Society Workshop*, vol. 2, pp. 711–720, December 2000.
- [22] M. Skolnik, *Introduction to Radar Systems*, 2nd ed. McGraw-Hill, 1980.
- [23] N. A. Goodman and D. Bruyere, "Optimum and decentralized detection for multistatic airborne radar," *IEEE Transaction on AES*, vol. 43, no. 2, pp. 806–813, April 2007.
- [24] R. Klemm, *Principles of Space-Time Adaptive Processing*. IEE Press, London, 2002.
- [25] S. M. Kay, *Fundamentals of Statistical Signal Processing: Detection Theory*, 1st ed. Prentice Hall PTR, 1993, vol. 2.
- [26] M. Barkat and P. K. Varshney, "Decentralized CFAR Signal Detection," *IEEE Transactions on Aerospace and Electronic Systems*, vol. 25, no. 2, pp. 141–149, March 1989.
- [27] R. Srinivasan, "Designing distributed detection systems," *IEE Proceedings-F, Radar and Signal Processing*, vol. 140, no. 3, pp. 191–197, June 1993.
- [28] R. Viswanathan and P.K.Varshney, "Distributed Detection with Multiple Sensors: Part I – Fundamentals," *Proceedings of the IEEE*, vol. 85, no. 1, pp. 54–63, January 1997.
- [29] R. S. Blum, S. A. Kassam, and H. Poor, "Distributed Detection with Multiple Sensors: Part II – Advanced Topics," *Proceedings of the IEEE*, vol. 85, no. 1, pp. 64–79, January 1997.
- [30] N. Levanon, *Radar Principles*. John Wiley & Sons, 1988.
- [31] F. C. Robey, D. R. Fuhrmann, E. J. Kelly, and R. Nitzberg, "A CFAR Adaptive Matched Filter Detector," *IEEE Trans. on Aerospace and Electronic Systems*, vol. 28, no. 1, January 1992.
- [32] M. W. L., "A STAP Overview," *IEEE Aerospace and Electronic Systems Magazine*, vol. 19, no. 1, January 2004.
- [33] N. F. E., *Radar Design Principals*, 2nd ed. McGraw-Hill, 1990.
- [34] M. Skolnik, *Radar Handbook*, 2nd ed. McGraw-Hill, 1990.